Vietnam Journal of Catalysis and Adsorption
Tạp chí xúc tác và hấp phụ Việt Nam

http://chemeng.hust.edu.vn/jca/

Construction of $NdFeO_3$ nanoparticles on reduced graphene oxide for an enhanced visible light assisted-Fenton degradation of organic pollutant in oily wastewater

Thi To Nga Phan*, Thi Hai Nam Chu

School of Chemical Engineering, Hanoi University of Science and Technology
**Email: nga.phanthito@hust.edu.vn*

ARTICLE INFO

Received: 30/3/2023
Accepted: 03/6/2023
Published: 30/6/2023

Keywords:

$NdFeO_3$, rGO, photo-Fenton, visible light, phenol

ABSTRACT

In this study, reduced graphene oxide (rGO) incorporated on $NdFeO_3$ (NFO/rGO) nanocomposite was successfully synthesized by using a facile hydrothermal method for photo-Fenton degradation of phenol in oily wastewater. The structural, elemental, morphological, optical property, and photo-Fenton performance of NFO/rGO nanocomposite were evaluated. From the characterizations, the prepared NFO/rGO nanocomposite showed a heterostructure between reduced graphene oxide (rGO) and $NdFeO_3$. In addition, the prepared NFO/rGO photocatalyst has efficient charge separation compared to that of pure NFO. The photo-Fenton catalytic activity of the NFO/rGO photocatalyst was investigated by phenol degradation under visible light irradiation, with a maximum removal efficiency of 94.3 % after 90 min. In contrast to pure NFO, the introduction of rGO could suggestively enhance the photo-Fenton catalytic activity by increasing the specific surface area and narrow band gap energy. The possible reaction mechanism was also discussed.

Introduction

Many environmental problems are brought on by industrialization, technological advancement, and social modernization. The many pollutants such as phenol and its derivatives that are incorporated into the groundwater supplies have extremely negative effects on the entire environment [1]. Humans have serious health problems as a result of untreated effluents from the textile, plastics, food, and petroleum industries that are dumped directly into the water system [2]. As a result, a variety of technologies have been used to eliminate wastewater effluents. Due to its effectiveness, environmental friendliness, and potential to reverse the existing environmental degradation, photo-Fenton catalysis stands out among the alternatives as the most promising one [3]. Perovskite materials with the ABO_3 formula (A = rare earth and B = transition metals) have recently attracted interest because their appealing use in numerous technological areas [4]. $NdFeO_3$ has attracted interest among different ABO_3 photocatalysts due to its compelling photocatalytic properties. Due to its low cost, good chemical stability, small band gap energy, $NdFeO_3$ has also been a prospective and well-known semiconductor photo-Fenton catalyst [5]. However, perovskites prepared by traditional techniques, such as hydrothermal, sol-gel, co-precipitation, etc., typically have low specific surface area and big particle size, which has a negative impact on their activity and contact efficiency with organics [6]. Many attempts have been made to overcome this by incorporating the

https://doi.org/10.51316/jca.2023.029

perovskites onto/into suitable supports, such as silica [7], gC_3N_4 [8], zeolite [9], and graphene [10]. Among the various supports, graphene have been found to be promising for a photocatalytic system because of their high surface area, excellent hydrophobicity, high electrical and thermal conductivity, electron mobility, chemical stability and mechanical strength [11]. Reduced graphene oxide (rGO) sheets appear more advantageous than graphene because it can catalyze the generation of •OH owing to the oxygen containing functional groups (i.e., carboxyl, hydroxyl, and epoxy groups) on the layered rGO surfaces [12]. Besides, through a range of potential chemical interaction mechanisms, such as bonding interaction, hydrophobic effect, and electrostatic interaction, rGO may enable high accessibility and interactions of reactants toward the surface active sites [13]. Through interactions, the large specific surface area and high affinity of rGO may promote the adsorption of organic molecules (suitable for decomposing pollutants). In addition, in order to improve the photocatalytic activity of pollutant degradation, rGO functions as an acceptor and transporter of electrons. This improves the efficiency of charge separation and prevents electron-hole (e-/h+) pair recombination.

This work reports the results of coupling rGO with $NdFeO_3$ *via* a facile impregnation method followed by calcination and evaluating its photo-Fenton-like activity in degradation of phenol under visible light. Various physicochemical properties of the synthesized samples were evaluated by several characterization techniques. Furthermore, the exposure of different radicals involved in the photo-Fenton catalytic mechanism is also examined by scavenger experiments. To the best of our knowledge, no such work has been previously published.

Materials and methods

Materials

Neodymium nitrate hexahydrate ($Nd(NO_3)_3{\cdot}6H_2O$; 99.9%), Iron nitrate nonahydrate ($Fe(NO_3)_3{\cdot}9H_2O$; 98 %), citric acid ($C_6H_8O_7{\cdot}H_2O$; ≥99.5%), hydrogen peroxide solution (H_2O_2, 30%), ammonium hydroxide solution (NH_4OH, 30%), graphite (C, fine powder), sulfuric acid (H_2SO_4, 98%), phosphoric acid (H_3PO_4, 85%), potassium permanganate ($KMnO_4$, 99%), ascorbic acid ($C_6H_8O_6$, 98%), and ethanol (C_2H_5OH, 95%) were purchased from Sigma-Aldrich. All chemicals were analytical grade and used as received without further purification.

Synthesis of GO and rGO

Graphene oxide (GO) was synthesized by the improved Hummers method [14]. Typically, 1 g of graphite powder was dissolved in 120 ml/14 ml of an H_2SO_4/H_3PO_4 solution. After 24 hours, 6 g of $KMnO_4$ was gradually added to the mixture. The resultant solution was then stirred at 40°C for 6 h before 30 ml of H_2O_2 (30%) was added. To obtain a sample of graphene oxide, the sample was centrifuged, washed, and stirred at 50°C for 3 h. The sample was then dried at 80°C for 12 h. Reduced graphene oxide (rGO) was created by reducing GO with ascorbic acid. Then, 0.5 g of GO was sonicated into 1 L of distillate. Then, add 5 g of ascorbic acid and stir the mixture for 8 h at 90 °C. The solid sample was then centrifuged, filtered, and repeatedly washed with distilled water and ethanol before being dried at 80 °C and then calcined at 600 °C in a N_2 environment. The sample that resulted was reduced graphene oxide (rGO).

Synthesis of $NdFeO_3$/rGO

$NdFeO_3$-doped reduced graphene oxide ($NdFeO_3$/rGO) was synthesized by impregnation and following by calcination method. Typically, 0.01 mol $Nd(NO_3)_3.6H_2O$, 0.01 mol $Fe(NO_3)_3.9H_2O$ and 0.02 mol citric acid was dissolved in a mixture of 10/20 mL of DI water/ethanol to form a homogeneous solution at ambient temperature. After adding 2 g rGO, the resulting suspension was stirred at room temperature for 3 h and then at 70 °C to evaporate the solvent, followed by drying at 80 °C and then calcination at 800 °C (heating rate of 2 °C/min from room temperature to 800 °C in air). The corresponding catalyst were named as NFO/rGO. For comparison, the sample, which was synthesized following the same above procedures in the absence of rGO, was denoted as NFO.

Characterizations of $NdFeO_3$/rGO

X-ray powder diffraction (XRD) pattern was measured on D8 Advance - Bruker diffractometer with Cu-Kα radiation with wavelength λ=1.54065 Å, scanning speed 0.02^0/s, 2θ range from 10^0 to 80^0. The surface morphology of the material was investigated by scanning electron microscopy (SEM) on the Zeiss 1555 VP-FESEM. Nitrogen adsorption-desorption isotherm was conducted at 77K on MICROMERITICS 2020.

https://doi.org/10.51316/jca.2023.029

Ultraviolet diffuse reflectance spectroscopy was measured on LAMBDA 750 UV/Vis/NIR system, PerkinElmer.

Measurement of photo-Fenton catalytic activity

Photo-Fenton catalytic activity of the sample was evaluated by adding 0.01 g NFO/rGO into 100 mL of 10 mg/L phenol aqueous solution in a double wall glass reactor equipped with a circulating water jacket to keep solution temperature at room temperature. Before photo-Fenton process, the suspension was magnetically stirred in dark for 60 min to reach an adsorption-desorption equilibrium of phenol onto NFO/rGO. A photo-Fenton reaction was started by introducing 1 mL H_2O_2 to the suspension along with turning on a Xenon lamp (CEL-HX F300) with a 400 nm cut-off filter to provide visible light for photo-Fenton degradation test. After that, 4 mL of the sample was taken from the suspension every 15 min and centrifuged for separation; the obtained supernatant was tested using Perkin Elmer Lambda 750 UV/Vis spectrometer to confirm the concentration of phenol. The degradation efficiency of phenol using the NFO/rGO sample was calculated as:

$$Degradation\ rate\ (\%) = \left(1 - \frac{C_t}{C_0}\right) \times 100\%$$

where C_0 and C_t are the concentration of phenol before and after time t in the photo-Fenton degradation.

The total photo-Fenton removal rate % was calculated using formula given below:

$$Removal\ rate\ (\%) = \left(1 - \frac{C_i}{C}\right) \times 100\%$$

where $\mathbf{C}$ is the concentration of phenol in the fresh solution before starting adsorption and C_i is the concentration of phenol at a given period of time during the adsorption – degradation process.

Results and discussion

Morphology analysis

The morphology of as-prepared photocatalysts was examined by scanning electron microscopy (SEM). As clearly shown (Fig. 1a), the NFO has an agglomerated sphere-like shape with various sizes in the range of 50 – 70 nm. It may be caused by adjusting lower solution pH in the present synthesis. Figure 1b showed SEM image of NFO/rGO sample. It can be seen that the sphere structure of NFO was retained and the NFO particles were dispersed on the graphene sheets. Additionally, The NFO/rGO sample also showed a clearly combined NFO nanosphere and rGO sheet with good contact. This contact allowed the electronic interaction between NFO nanoparticles and graphene sheets and could be potentially beneficial for effective separation of charge carriers and enhancing its photo-Fenton catalytic activity.

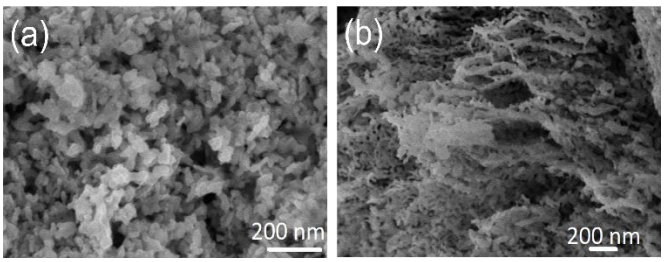

Figure 1: SEM images of (a) NFO and (b) NFO/rGO

XRD analysis

The purity of the samples was examined by powder X-ray diffraction (XRD). Fig. 2 showed the XRD patterns of the GO, rGO, $NdFeO_3$, and $NdFeO_3$/rGO composites. As can be seen from Fig. 2 that GO presented a single and broad diffraction peak at a 2θ of 11.3 °, having an interlayer distance of 8.97 Å, indicating that most of the graphite powder was oxidized into GO. Meanwhile, the $NdFeO_3$ and $NdFeO_3$/rGO samples showed the similar diffraction peaks match perfectly to the orthorhombic perovskite $NdFeO_3$ (JCPDS No. 37-1493) [15]. For $NdFeO_3$/rGO sample, characteristic diffraction peak at 11.3 ° disappeared implying the successful reduction of GO to reduced graphene (rGO) in the final $NdFeO_3$/rGO sample.

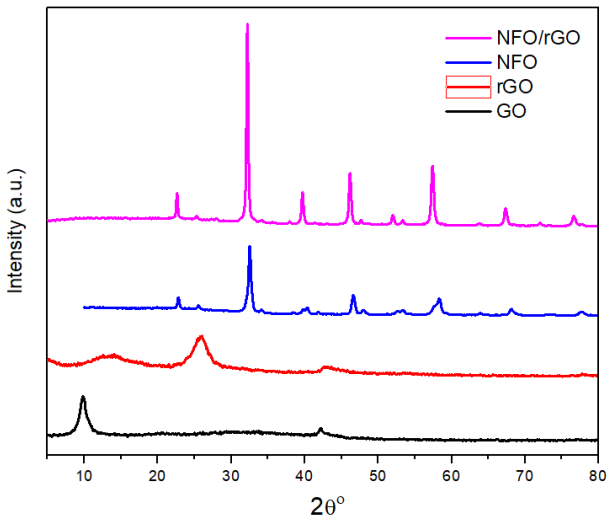

Figure 2: XRD pattern of GO, rGO, NFO, and NFO/rGO

https://doi.org/10.51316/jca.2023.029

BET specific surface area

The BET specific surface areas of pure NFO and the NFO/rGO samples are summarized in Table 1. The specific surface area of pure NFO sample was found to be 8.9 m^2/g, which could be attributed to the fact that hydrothermal synthesis can cause a small specific surface area of perovskites [16]. As is clearly seen, the BET specific surface area greatly increased with incorporating of rGO and the NFO/rGO sample showed much higher BET specific surface area as compared with pure NFO sample. It can be explained by the average densities of samples. The planar density of graphene is 1.5 mg/cm^2 while the density of $NdFeO_3$ is 7.01 g/cm^3 [17, 18] . Therefore, the average densities of NFO/rGO sample decreased when doping with graphene, resulting in the increase of its BET specific surface area. Similar observations were recently reported for Co-Fe-codoped graphene-$LaCrO_3$ [19] and $LaNiO_3$-loaded nitrogen-doped reduced graphene oxide [20]. The BET surface areas of NFO/rGO was much improved and it would have a great impact on photo-Fenton catalytic activity.

Table 1: Structural property of NFO and NFO/rGO samples

Sample	S_{BET} (m^2/g)	Pore volume (cm^3/g)	Average pore size (nm)
NFO	8.9	0.05	27.63
NFO/rGO	20.1	0.089	18.25

Optical property

UV-Vis absorption spectra in the wavelength range of 300- 800 nm of rGO, NFO, and NFO/rGO samples were studied and the results were illustrated in Fig. 3a. It was easy to see that NFO sample exhibited strong absorption peaks in the visible region (400 - 800 nm) while rGO was hardly absorb the visible light, as shown in Fig. 3a. However, the incorporation of rGO into NFO structure significantly affected the optical absorption property for the NFO/rGO sample. As compared to the pure NFO, the absorption peak in the visible region was improved for the NFO/rGO sample. The optical band gap of the material can be determined from the reflectance spectral data according to the Kubelka-Munk equation. The optical band gap is determined based on the relationship between hν (energy corresponding to each wavelength) and the coefficient α, which depends on F(R) – the Kubelka-Munk function according to the expression [21]:

$$F(R) = \frac{(1-R)^2}{2R} \quad (1)$$

The relationship between $[(F(R).h\nu)^2]$ and hν in the allowed direct electron transition is shown in Fig. 3b. The optical band gap energy of the NFO and NFO/rGO was found to be 2.67 and 2.52 eV, respectively. The narrow band gap energy of the NFO/rGO sample indicated that the NFO/rGO can act as photocatalyst activating in the visible light region. Obviously, the results indicated that reduced graphene oxide has a significant impact on the optical characteristics of the as-prepared sample, indicating that the addition of rGO increased the absorption of visible light and was anticipated to improve photo-Fenton catalytic activity when exposed to visible light.

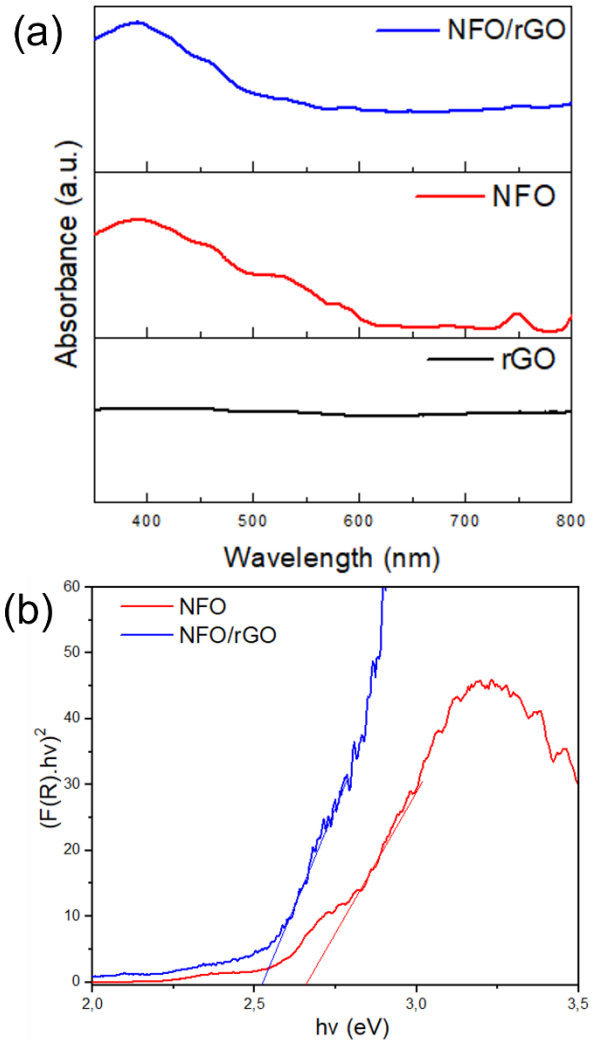

Figure 3: (a) UV-Vis absorption spectra of rGO, NFO, and NFO/rGO and (b) the plot of $(F(R)h\nu)^2$ versus hν

Photo-Fenton degradation of phenol

Figure 4 showed the removal of phenol using no photocatalyst, rGO, NFO, and NFO/rGO *via* adsorption in dark condition and photo-Fenton degradation under visible light. As can be seen clearly from the Fig. 4 that under visible light illumination, the test using no photocatalyst illustrated hardly phenol degradation without H_2O_2 and 8.6 % in the presence of H_2O_2. The rGO sample adsorbed 33.5 % of phenol in dark condition when reaching equilibrium due to the π- π interaction between rGO and phenol [22]. After exposure to visible light, it slowly removed ~11 % of phenol after 90 min. This showed a higher total phenol removal rate compared to the amount of phenol degrading in the presence of light and H2O2 without the use of any materials. This suggests that rGO is not an effective catalyst for photo-Fenton degradation of phenol. Meanwhile, the sample of NFO removed 1.2 % and 57.8 % of phenol *via* adsorption and photo-Fenton degradation, respectively. Noting that, the incorporating of NFO in rGO reduced the adsorption capacity of the rGO sample; however, it considerably enhanced photo-Fenton catalytic activity of as-prepared sample NFO/rGO.

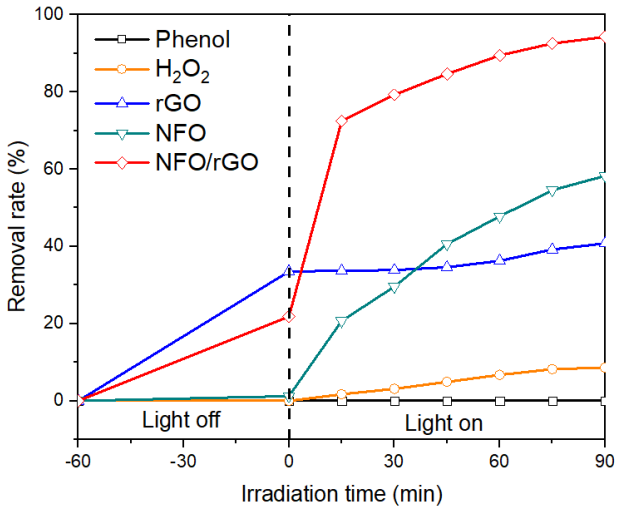

Figure 4: Photo-Fenton degradation of phenol as a function of irradiation time by using NFO/rGO (reaction conditions: phenol concentration = 10 mg/L; photocatalyst dosage = 1.0 g/L; H_2O_2 concentration = 10 mM; solution pH = 6; temperature = 25 °C)

The total phenol removal *via* degradation using NFO/rGO was the highest compared to that of two samples rGO and pure NFO, being 94.3 %. Interestingly, the total removal rate of phenol obtained with NFO/rGO (94.3 %) was significantly greater than that using the pure NFO sample (57.8 %). This might be due to the enhancement of dark adsorption using NFO/rGO 21.8 %) as compared with NFO (~1.2 %), which could largely facilitate the subsequent photo-Fenton degradation under visible light. Most importantly, the use of rGO as the support in the synthesis of NFO-based photocatalyst caused an increase in specific surface area and active sites which are accessible to phenol for degradation.

The photo-Fenton catalysis mechanism of organics degradation under visible light radiation using NFO/rGO photocatalyst could be proposed to take place through two simultaneous processes, including the Fenton reaction and the photocatalysis. On the one hand, during the Fenton reaction, the Fe atom on the surface of the NFO/rGO sample (denoted as Fe^{3+}) react with H_2O_2 to generate hydroxyl radicals ▪OH (Eqs. 2-5):

$Fe^{3+} + H_2O_2 \rightarrow Fe^{3+}\ H_2O_2$ (2)

$Fe^{3+}\ H_2O_2 \rightarrow Fe^{2+} + HO_2\blacksquare + H^+$ (3)

$Fe^{3+} + HO_2\blacksquare + H^+ \rightarrow Fe^{2+} + O_2 + 2H^+$ (4)

$Fe^{2+} + H_2O_2 \rightarrow Fe^{3+} + \blacksquare OH + OH^-$ (5)

On the other hand, the photocatalysis reaction starts when the NFO/rGO particles absorb photons from visible light source, which makes the electrons excited and moved from the valence band (VB) to the conduction band (CB) in NFO/rGO structure. Noting that, at the position where the electrons are ejected, holes (h+) with positive charge and electron (e-) with negative charge will be created on the NFO/rGO surface (Eq. 6). These (e-) will then be trapped by H_2O_2 molecules and generate ▪OH free radicals (Eq. 7) [23].

NFO/rGO → NFO/rGO (e^- + h^+) (6)

$H_2O_2 + e^- \rightarrow \blacksquare OH + OH^-$ (7)

Obviously, hydroxyl radicals (▪OH) are continuously generated and combined with phenol molecules to directly oxidize phenol presenting in wastewater under visible light irradiation to form degradation products, as Eq.8 [24]:

▪OH + phenol → Degradation products (8)

Conclusions

The photocatalyst $NdFeO_3$ incorporated with reduced graphene oxide (rGO) was successfully prepared by the impregnation method and following by calcination. The characterization results revealed that NFO/rGO sample showed larger specific surface area and narrower bandgap energy compared to pure NFO. It also exhibited higher total removal rate of phenol (94.3 %) from water; which was contributed to dark

adsorption (21.8 % in 60 min) and photo-Fenton degradation (92.7 % in 90 min in the presence of 10 mM H_2O_2, 1 g/L NFO/rGO photocatalyst and pH of 6). The proposed mechanism suggested that in the photo-Fenton process, the hydroxyl radicals were the main active species. The good photo-Fenton degradation performance might enable promising practical application of NFO/rGO as a visible-light-assisted photo-Fenton catalyst for removal of phenol from wastewater.

Acknowledgement

This research is funded by Vietnam Ministry of Education and Training under grant number B2021-BKA-15.

References

1. Kumar, A., et al., Mater. Chem. Frontiers 1(11) (2017) 2391-2404. https://doi.org/10.1039/C7QM00362E
2. Sun, J., et al., J. Colloid Inter. Sci. 588 (2021) 19-30. https://doi.org/10.1016/j.jcis.2020.12.043
3. Ebrahiem, E.E., M.N. Al-Maghrabi, and A.R. Mobarki, Arabian J. Chem. 10 (2017) S1674-S1679. https://doi.org/10.1016/j.arabjc.2013.06.012
4. Kumar, A., A. Kumar, and V. Krishnan, Acs Catal. 10(17) (2020) 10253-10315. https://doi.org/10.1021/acscatal.0c02947
5. Prabagar, J.S., et al., Mater. Today: Proceedings 75 (2023) 15-23. https://doi.org/10.1016/j.matpr.2022.10.230
6. Phan, T.T.N., et al., J. Environ. Manage. 233 (2019) 471-480. https://doi.org/10.1016/j.jenvman.2018.12.051
7. Phan, T.T.N., et al., RSC Adv. 8(63) (2018) 36181-36190. https://doi.org/10.1039/C8RA07073C
8. Wang, L., et al., J. Environ. Chem. Eng. 10(5) (2022) 108330. https://doi.org/10.1016/j.jece.2022.108330
9. Nga, P.T.T., et al., Vietnam J. Chem. 60(1) (2022) 76-83. https://doi.org/10.1002/vjch.202100082
10. Farhadi, A.R.K., et al., J. Taiwan Ins.Chem. Eng. 120 (2021) 77-92. https://doi.org/10.1016/j.jtice.2021.03.021
11. Venkatesh, G., et al., Colloids Surf. A: Physicochem. Eng. Aspects 629 (2021) 127523. https://doi.org/10.1016/j.colsurfa.2021.127523
12. Xu, D., et al., App. Catal. B: Environ. 164 (2015) 380-388. https://doi.org/10.1016/j.apcatb.2014.09.05
13. Zubir, N.A., et al., Chem.l Commu. 51(45) (2015) 9291-9293. https://doi.org/10.1039/C5CC02292D
14. Justh, N., et al., J. Thermal Anal. Calorimetry, 131 (2018) 2267-2272. https://doi.org/10.1007/s10973-017-6697-2
15. Wang, Y., et al., Mater. Let. 60(13-14) (2006) 1767-1770. https://doi.org/10.1016/j.matlet.2005.12.015
16. Phan, T.T.N., et al., J. Chem. 2021 (2021) 1-11. https://doi.org/10.1155/2021/5841066
17. Karpov, O., M. Tomkovich, and E. Tugova, Russian J. General Chem. 88 (2018) 2133-2138. https://doi.org/10.1134/S1070363218100171
18. Wang, Z., et al., Nano Res. 3 (2010) 748-756. https://doi.org/10.1007/s12274-010-0041-5
19. Aamir, M., et al., J. Mole. Liquids 322 (2021) 114895. https://doi.org/10.1016/j.molliq.2020.114895
20. Yuasa, M., et al., J. Appl. Electrochem. 49 (2019) 1055-1067. https://doi.org/10.1007/s10800-019-01350-x
21. Albadi, Y., et al., Inorganics 9(5) (2021) 39. https://doi.org/10.3390/inorganics9050039
22. Meng, X., Li, Z., & Zhang, Z., Chemosphere 198 (2018) 1-12. https://doi.org/10.1016/j.chemosphere.2018.01.070
23. Huang, T., et al., J. Environ. Chem. Eng. 8(5) (2020) 104384. https://doi.org/10.1016/j.jece.2020.104384
24. Phan, T.T.N., et al., Appl. Surf. Sci. 491 (2019) 488-496. https://doi.org/10.1016/j.apsusc.2019.06.133